Int. J. Electrochem. Sci., 17 **(2022)** Article Number: 22105, doi: 10.20964/2022.10.36

International Journal of
ELECTROCHEMICAL
SCIENCE
www.electrochemsci.org

Influence of Temperature on the Corrosion Behavior of 18Mn–18Cr Austenitic Stainless Steel in 3.5 wt.% NaCl Solution

Junping Chen[1], *Qiongyu Zhou*[2,3,*], *Yu Liu*[3], *Yanhui Ma*[1],*Jianfen Yin*[1], *Te Hu*[2] , *Yuanyuan Li*[2*]

[1] North China Electric Power Institute Co.,Ltd, Beijing 100045, *China*
[2] School of Materials Science and Energy Engineering, Foshan University, Foshan 528000, China
[3] Research Institute of Automobile Parts Technology, Hunan Institute of Technology, Hengyang, 421002, PR China
[*]E-mail: zhouzhouqiongyuxf@126.com; liyuanyuan@wust.edu.cn

Received: 9 May 2022 / *Accepted:* 21 June 2022 / *Published:* 10 September 2022

18Mn–18Cr austenitic stainless steels (P900) are usually applied in manufacturing of rotors and coil retaining rings, which may be served in a high temperature environment. In this paper, the influence of temperature on the corrosion behavior of 18Mn–18Cr austenitic stainless steel in 3.5 wt.% NaCl solution has been investigated by the OCP monitoring, potentiodynamic polarization, potentiostatic polarization, electrochemical impedance spectroscopy (EIS) and Mott–Schottky analysis. Results show that the general corrosion resistance and pitting corrosion resistance of 18Mn–18Cr austenitic stainless steels would both decrease with the increase of temperature, based on that the decreased values of E_{ocp}, E_{corr} E_{pit}, i_{corr} and impedance. Besides, the pitting incubation period of 18Mn–18Cr austenitic stainless steels is sensitive to the temperature (about 1711 s at 40 ℃ and less than 100s at 45 ℃). In addition, the passive films formed on 18Mn–18Cr austenitic stainless steel exhibit n-type semiconductor characteristic. The donor concentrations (N_D) increase with the increase of temperature, which results in the reduced corrosion resistance at a higher temperature.

Keywords: 18Mn–18Cr stainless steels, Corrosion resistance, Passive film, n-type semiconductor

1. INTRODUCTION

Given the fact that the cost caused by corrosion has been over 3% of the world's gross, corrosion has become an unavoidable topic for metallic materials [1, 2]. Tremendous efforts have been made to meet the challenge of corrosion failure [3, 4]. Thus, exploitation of practical materials, which owns high corrosion resistance and acceptable price, has drawn lots of attention [5-7].

Stainless steel, an iron based alloy with at least 10.5 wt.% chromium and other elements (such as Ni, Mn et al.), is a typical corrosion-resistant material. There are various stainless steels which have been successfully used in industry, power sector, space aerospace, oceanographic engineering [8, 9]. It

can be established that the oxides/hydroxides films (passive films) formed on the surface of stainless steels could shield the substrate from aggressive ions [10-12]. Therefore, the corrosion behavior of stainless steels is mainly attributed to the formation and collapse of the protective passive films [13]. Once the passive films have been damaged, localized corrosion (pitting corrosion, stress corrosion etc.) is prone occurred in the damaged areas without the protection of passive film [14]. Numerous previous studies demonstrate that the corrosion of stainless steels are highly associated with the material characteristics (chemical composition, microstructure, etc.) and environmental factors (temperature, pH values, fluid velocity, oxygen content, aggressive ion species and content) [15-19]. Among these factors, the temperature plays a significant role in the growth and dissolution of the passive films [16, 20]. Thus, the influence of temperature on the corrosion behavior is an important aspect in the study of corrosion resistance of stainless steel [21].

18Mn–18Cr austenitic stainless steels (P900) have been successfully applied in the power industry for manufacturing of rotors and coil retaining rings, due to their high strength and outstanding corrosion resistance in moisture environment [22-24]. Generally, the operation of generator sets would result in increase of temperature. [25]. Hence, the 18Mn–18Cr austenitic stainless steels component may be served in high temperature environment. It is well know that the increase of temperature has a profound effect on the pitting initiation and re-passivation behavior, which is the critical factor for the corrosion resistance of stainless steels. However, the study of the influence of temperature on the corrosion behavior of 18Mn–18Cr austenitic stainless steel has not been progressed [16, 20-21]. Therefore, the corrosion behavior (especially pitting corrosion resistance) of 18Mn–18Cr steel caused by temperature variations has been investigated in this study by using a variety of corrosion electrochemical techniques, such as open circuit potential monitoring, potentiodynamic polarization, potentiostatic polarization, electrochemical impedance spectroscopy and Mott-Schottky analysis.

2. EXPERIMENTAL

Commercial 18Mn–18Cr austenitic stainless steel samples (11 mm × 11 mm × 2 mm) used in this paper were drawn from the coil retaining rings in generator set (State Grid Corporation of China) by electrical discharge machining. The chemical composition was detected by inductively coupled plasma atomic emission spectrometer (ICP-AES, Optima-7000DV, Thermofisher) and the results are listed in Table 1. The samples were ground with SiC paper (from 80 to 2000 grit, sequentially), polished with 0.1 μm diamond powder. Then, the polished samples were cleaned with acetone, deionized water and then dried in cool air. Afterthat, the samples were encapsulated by epoxy to confirm that the exposed area is 10 mm × 10 mm.

Table 1. Chemical composition of 18Mn–18Cr stainless steel used in this paper (wt.%).

Mn	Cr	Si	Ni	Mo	S	P	Fe
19.07	18.21	0.58	0.56	0.08	0.03	0.02	Bal.

The electrochemical tests were conducted on a PARSTAT VersaSTAT 3F workstation with a classical three-electrode electrochemical cell, which contains Pt sheet (20 mm×20 mm, counter electrode), saturated-calomel electrode (SCE, reference electrode) and 18Mn–18Cr stainless steel (working electrode). The test solution was 3.5 wt. % NaCl solution (open to air), which was prepared by analytical grade chemicals and deionized water. The solution temperature is controlled by thermostat water bath and set to be 25 ℃, 45 ℃, 60 ℃, 80 ℃， respectively. The potentiodynamic polarization measurements were starting at -0.5 V vs. open circuit potential (OCP) and ended at the potentials when current density rose to 1 mA cm^{-2}, with a scan rate of 10 mV min^{-1}. The EIS tests were executed at the open circuit potential (OCP) in the frequency range of 10^5 Hz ~10^{-2} Hz, by using a 10 mV AC stimulus signal. Mott–Schottky plots were tested in the potential range from -0.4V to 0.8 V, with a scan rate of 0.05 V s^{-1}, at the applied frequency of 10^3 Hz. In addition, Zsimpwin software was employed to interprete the EIS results. The potentiostatic polarization was carried out at 0.15 V for 120 min and the test temperature was set to be 25 ℃, 35 ℃, 40 ℃, 45 ℃, respectively.

3. RESULTS AND DISCUSSION

3.1 Open circuit potential (OCP) monitoring

The OCP values vs. time (E_{ocp}-t) curves for the 18Mn–18Cr austenitic stainless steel immersed in 3.5 wt. % NaCl solution, obtained at the temperature of 25, 45, 60 and 80 ℃, are shown in Fig. 1. It can be found that the OCP values are fluctuant in the initial period of immersion, which is due to the oxide/passive films on the surface of 18Mn–18Cr austenitic stainless steel destroyed and formed continuously [26]. In addition, the degree of fluctuation for OCP values in the initial period of immersion intensifies with the increase of temperature.

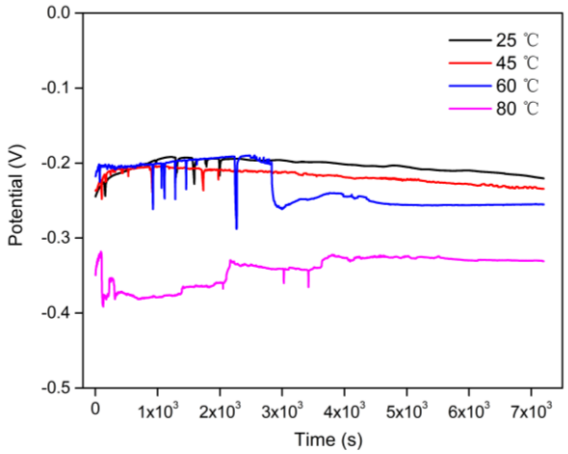

Figure 1. E_{ocp}-t curves for the 18Mn–18Cr austenitic stainless steel immersed in 3.5 wt.% NaCl solutions at different temperatures

After 4000s of immersion, the OCP values would tend to be stable, meaning that the dynamic equilibrium between the formation and dissolution of the oxide/passive films has been achieved [27]. In addition, the OCP values after a long time of immersion decrease with the increase of temperature (~221 mV for 25 ℃, ~234 mV for 45 ℃, ~254 mV for 60 ℃, ~331 mV for 80 ℃, respectively), indicating that the decrease of thermodynamics stability.

3.2 Polarization curves analysis

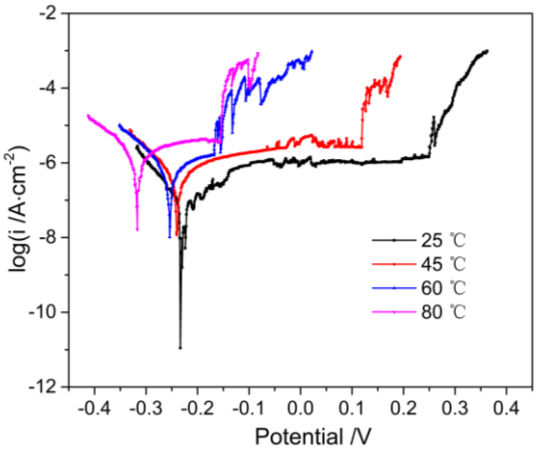

Figure 2. Potentiodynamic polarization curves of the 18Mn–18Cr austenitic stainless steel in 3.5 wt. % NaCl solutions at different temperatures, with a scan rate of 10 mV/min.

Fig. 2 shows the potentiodynamic polarization curves of the 18Mn–18Cr austenitic stainless steel. The corrosion electrochemical parameters extracted from Fig. 2 are listed in Table 2. Clearly, there exists typical passivation characteristics in all potentiodynamic polarization curves, in where the current densities are independent of potentials [28]. Besides, all polarization curves change directly into the passive region from the corrosion potential (E_{corr}), without an active to passive transition, confirming that the 18Mn–18Cr austenitic stainless steel owns superior passive properties in 3.5 wt. % NaCl solution [29]. With the increase of temperature, both the E_{corr} and E_{pit} tend to be more negative, and the i_{corr} values increase (shown in Table 2). These results indicate that the general corrosion resistance and pitting corrosion resistance of 18Mn–18Cr austenitic stainless steel are sensitive to the temperature and would decrease at a higher temperature.

Table 2. The corrosion electrochemical parameters obtained from the potentiodynamic polarization curves in Fig.2

Temperature(℃)	E_{corr} (mV)	i_{corr} (μA cm^{-2})	E_{pit} (mV)	E_{pit}-E_{corr} (mV)
25	-232	0.06	249	481
45	-240	0.23	116	356
60	-255	0.39	-169	86
80	-314	1.04	-153	161

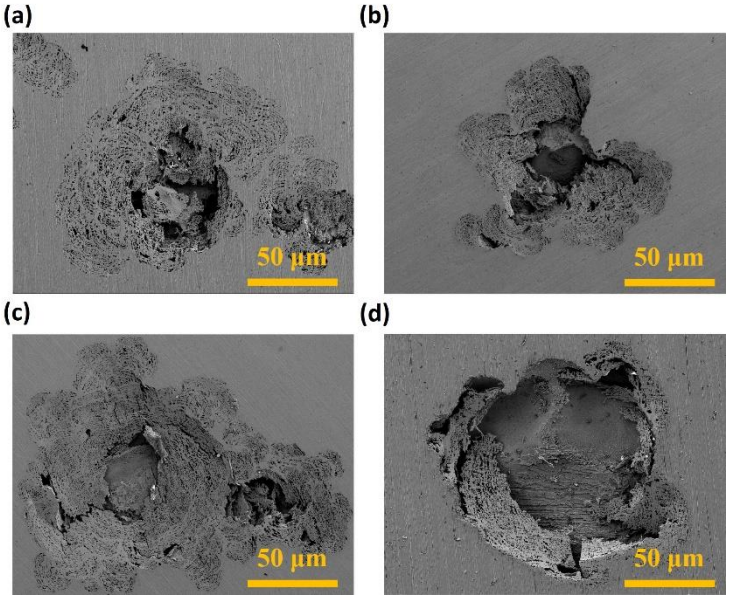

Figure 3. SEM morphologies of the 18Mn–18Cr austenitic stainless steel after the polarization tests in 3.5 wt. % NaCl solutions at different temperatures: (a) 25 ℃, (b) 45 ℃, (c) 60 ℃， (d) 80 ℃.

The SEM morphologies of the 18Mn–18Cr austenitic stainless steel after the polarization tests in 3.5 wt. % NaCl solutions are displayed in Fig. 3. There are typical pits which displayed rough and porous bottom formed on the surface of 18Mn–18Cr austenitic stainless steel. These appearances are exactly similar to that formed the surface of numerous austenitic stainless steels [30, 31]. Furthermore, it can be found that the radius and depths of the pits are increase with the increase of temperature.

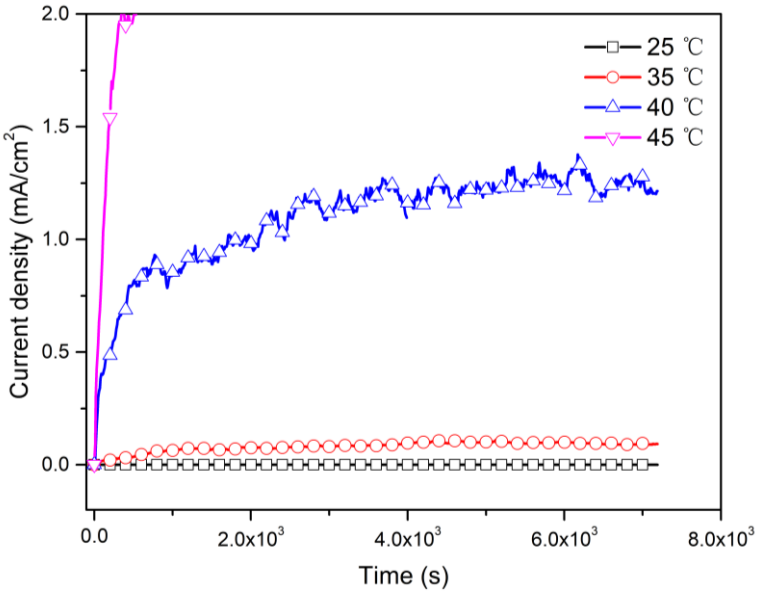

Figure 4. Current density versus time records of the 18Mn–18Cr austenitic stainless steel under potentiostatic polarization (0.15 V) at different temperatures in 3.5 wt. % NaCl solutions

The potentiostatic polarization has been used to thoroughly investigate the pitting sensitivity of 18Mn–18Cr austenitic stainless steel in 3.5 wt. % NaCl solutions is exhibited in Fig. 4. As shown, the current densities are fairly stable and quite small at 25 ℃ and 35 ℃ (~0.2 μA/cm^2 for 25 ℃ and ~0.1 mA/cm^2 for 35 ℃), indicating that compact passive films will be formed on the surface of 18Mn–18Cr austenitic stainless steel and can provide protective effects. While the current densities increase rapidly with the increase of polarization time at the temperature of 40 ℃ and 45 ℃. When the temperature is 40 ℃, the current densities increases to 1 mA/cm^2 at 1711 s. It means that pitting incubation period of 18Mn–18Cr austenitic stainless steel at 40 ℃ is about 1711 s, over which the formed passive films will be prone to local breakdown and result in pitting corrosion. When the temperature is 45 ℃, the pitting incubation period is less than 100s (shown in Fig. 4). The main reason for this phenomenon is that the activity and transfer of chloride ion will be promoted by the increase of temperature, which is generally considered to be extremely adverse for the passivating [32].

3.3 EIS analysis

EIS, which can affirm electrochemical states at the electrode/electrolyte interface without destructive, are employed to understand the corrosion mechanisms of passive films on the surface of 18Mn–18Cr austenitic stainless steel [33]. Fig. 5 shows the EIS spectra of the 18Mn–18Cr austenitic stainless steel at different temperatures in 3.5 wt. % NaCl solutions at the open circuit potentials. As shown, the impedance values (|Z|), which is revealed by the radius of the unfinished semicircle, decrease with the increase of temperature (Fig. 5a). In addition, relatively stabilized phase angles (70-85°) at the medium-low frequencies can be observed in Fig. 5b. This capacitive response relates to the presence of protective passive films [2]. These results are highly inconsistent with that obtained from the OCP monitoring and potentiodynamic polarization curves.

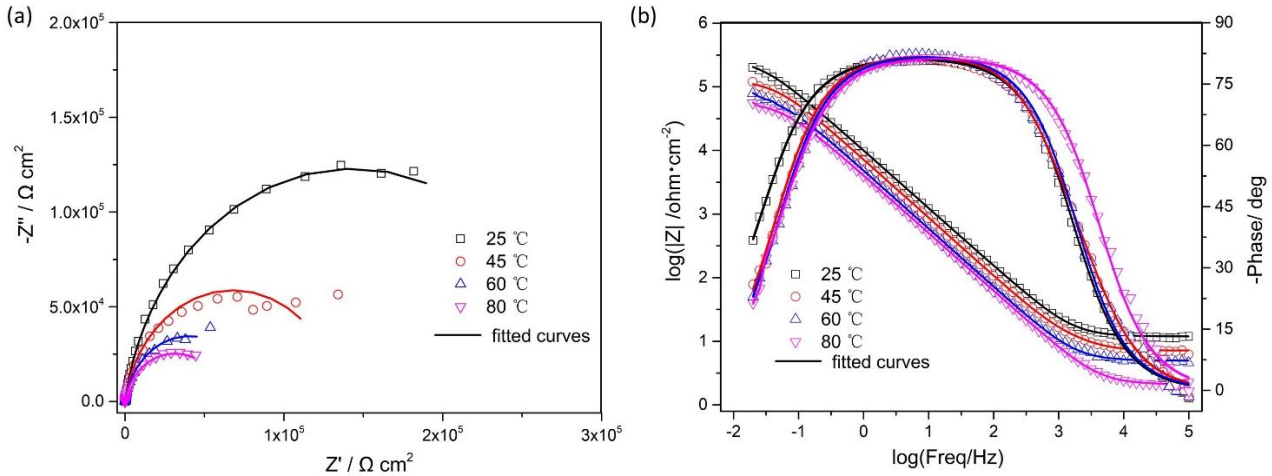

Figure 5. EIS spectra of the 18Mn–18Cr austenitic stainless steel at different temperatures in 3.5 wt. % NaCl solutions at the open circuit potentials (a: Nyquist plots, b: bode-phase plots)

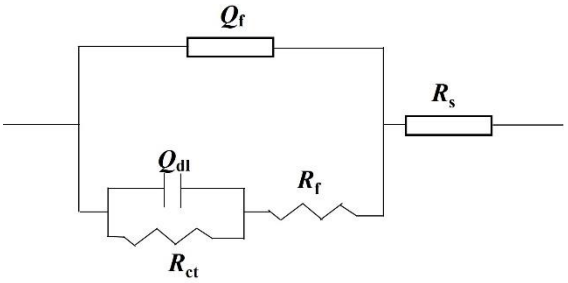

Figure 6. The used EEC for fitting the EIS spectra

In addition, an electrical equivalent circuit (EEC), which is displayed in Fig. 6, has been used to fit the experimental data and the results are list in Table 3. In the EEC, R_s, R_f and R_{ct} represent solution resistance, charge-transfer of the passive films on the surface and faradic resistance. Q_f and Q_{dl} represent the constant phase elements (CPEs), which can be used to account for the frequency dispersion caused by surface heterogeneity [33].

Table 3. The equivalent circuit parameters for EIS spectra of the 18Mn–18Cr austenitic stainless steel

T (°C)	R_s (Ω cm^2)	Q_f-Y_0 ($\mu\Omega^{-1}$ cm^{-2} s^n)	n_1	R_f (kΩ cm^2)	Q_{dl}-Y_0 ($\mu\Omega^{-1}$ cm^{-2} s^n)	n_1	R_{ct} (kΩ cm^2)	Σc^2 ($\times 10^{-3}$)
25	11.5	0.11	0.94	431	7.9	0.87	288	1.14
45	7.0	0.19	0.93	212	7.6	0.89	136	3.07
60	4.9	0.39	0.92	81	6.5	0.88	92	1.37
80	2.1	0.47	0.91	59	6.1	0.86	83	1.05

The chi-square values (Σc^2) are very small (~10^{-3} order of magnitudes) and the fitted curves match very well with the experimental EIS data (Fig. 5), confirming the good fitting quality. The proportionality factor for CPE impedance (Q_f-Y_0) values, which is inverse proportion to the passive film thickness (δ), are gradually increasing with the increase of temperature, meaning that the thickness (or quality) of passive film decreased [3]. Besides, both the R_f and R_{ct} values decrease with temperature. It demonstrates that the increase of temperature would lead to reduce the quality of the passive films formed on the 18Mn–18Cr austenitic stainless steel.

3.4 Mott–Schottky analysis

Generally, the passive films can act as barrier layers to prevent corrosion. In this aspect, the charge transport characteristic of the passive films formed on the surface of stainless steels, which usually exhibit semi-conductor properties, are particularly important for their corrosion resistance [34]. According to the Mott-Schottky theory, the space charge capacitance (C_{sc}) of the semiconductor for n-

type semiconductor p-type semiconductor could be expressed as equation (1) and equation (2), respectively.

$$\frac{1}{C_{SC}^2} = \frac{2}{\varepsilon\varepsilon_0 q N_D}(E - E_{fb} - \frac{kT}{e}) \quad (1)$$

$$\frac{1}{C_{SC}^2} = \frac{-2}{\varepsilon\varepsilon_0 q N_A}(E - E_{fb} - \frac{kT}{e}) \quad (2)$$

Where N_D, N_A and E_{fb} represent the donor concentrations, acceptor concentrations and flat-band potential, respectively. The ε is the dielectric constant of the formed passive film, which can be assumed as 12 for stainless steel [35]. Other constants such as vacuum permittivity (ε_0), electron charge (e) and Boltzmann constant (k) are 8.854 $\times 10^{12}$ F m^{-1}, 1.6×10^{19} C and1.38×10^{23} J K^{-1}, respectively.

Fig. 7 shows the Mott-Schottky plots of the passive films formed on the surface of the 18Mn–18Cr austenitic stainless steel at different temperatures in 3.5 wt. % NaCl solutions. Obviously, all the Mott-Schottky plots of the 18Mn–18Cr austenitic stainless steel show positive slopes, indicating that the formed passive films are n-type semiconductor. The N_D values calculated according to equation (1) are 4.13×10^{19} , 5.01×10^{19}, 8.91×10^{19}, 9.77×10^{19} cm^{-3} for the temperature of 25 ℃, 45 ℃, 60 ℃, 80 ℃, respectively. The point defect model (PDM), which is firstly proposed by D.D. Macdonald, claims that the formation and transport of vacancies (should be donors in this paper) at metal/film interface would contribute to passive films breakdown [6, 36, 37]. Therefore, the reduced corrosion resistance of 18Mn–18Cr austenitic stainless steel at a higher temperature must be caused by the increased donor concentrations.

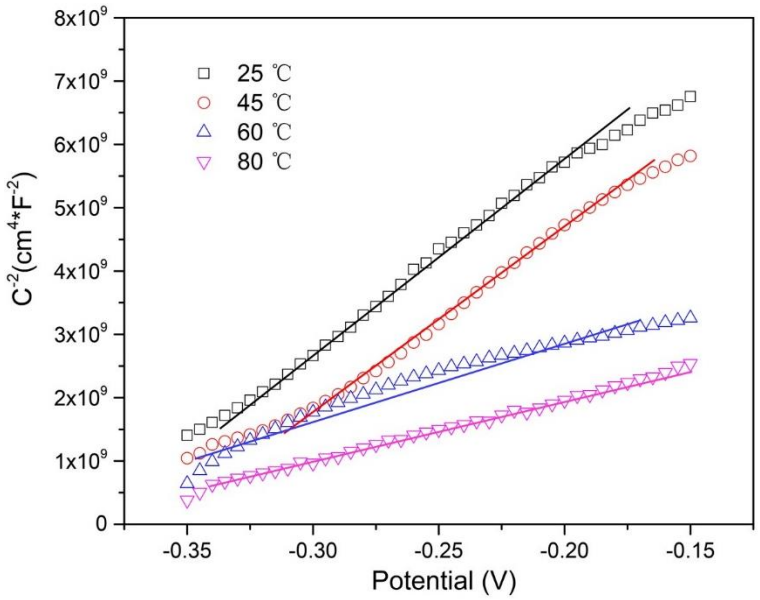

Figure 7. Mott-Schottky plots of the passive films formed on the surface of 18Mn–18Cr austenitic stainless steel at different temperatures in 3.5 wt. % NaCl solutions

4. CONCLUSIONS

In this work, the influence of temperature on the corrosion behavior of 18Mn–18Cr austenitic stainless steel in 3.5 wt.% NaCl solution has been studied by using OCP monitoring, potentiodynamic polarization, potentiostatic polarization, EIS and Mott–Schottky analysis. Conclusions could be drawn as follows:

(1) The general corrosion resistance and pitting corrosion resistance of 18Mn–18Cr austenitic stainless steel would decrease with the increase of temperature, based on that the E_{ocp}, E_{corr} E_{pit} become more negative, and the i_{corr} decrease at a higher temperature.

(2) Increase of temperature will shorten the pitting incubation period of 18Mn–18Cr austenitic stainless steel, which is 1711 s at 40 ℃ and less than 100s at 45 ℃.

(3) EIS results illustrate the thickness of passive film, R_f and R_{ct} values decrease with the increase of temperature, resulting in the decreased impedance values.

(4) The passive films formed on 18Mn–18Cr austenitic stainless steels exhibit n-type semiconductor characteristic. The N_D values increase with the increase of temperature, which may result in the decrease of corrosion resistance.

ACKNOWLEDGEMENTS
This work is financially supported by the Guangdong Basic and Applied Basic Research Foundation (2020A1515110818) and Key Scientific and Technological Project of Foshan City (1920001000409).

References

1. S. Ding, T. Xiang, C. Li, S. Zheng, J. Wang, M. Zhang, C. Dong and W. Chan, Mater. Des. 117 (2017) 280–288.
2. Q. Zhou, S. Sheikh, P. Ou, D. Chen, Q. Hu and S. Guo, *Electrochem. Commun., 98* (2019) 63-68.
3. H. Luo, Z. Li, A. M. Mingers and D. Raabe,. *Corros. Sci.,* 134 (2018) 131-139.
4. Q. Zhou, Y. Wang, H. Wu, Q. Zhong and J. Jiang, *Surf. Coat. Technol*., 207 (2012) 503-507.
5. J. Gao, J. Tan, X. Wu and S. Xia, *Corros. Sci.*, *152* (2019) 190-201.
6. D. D. Macdonald, *Electrochim. Acta,* 56 (2011)1761–1772
7. Y. Shi, B. Yang, X. Xie, J. Brechtl, K. A. Dahmen and P. K. Liaw, Corros. Sci. 119 (2017) 33–45
8. B. Zhang, S. Hao, J. Wu, X. Li, C. Li, X. Di and Y. Huang,. *Mater. Charact. 131* (2017) 168-174.
9. L. Chang, L. Volpe, Y. L. Wang, M. G. Burke, A. Maurotto, D. Tice, S. Lozano-Perez and F. Scenini,. *Acta Mater.*, *165* (2019) 203-214.
10. R. Jiang, Y. Wang, X. Wen, C. Chen and J.Zhao, *Appl. Surf. Sci*., *412* (2017) 214-222.
11. C. Örnek, M. Långberg, J. Evertsson, G. Harlow, W. Linpé, L. Rullik, F. Carlà, R. Felici, E. Bettini, U. Kivisäkk, E. Lundgren and J. Pan, *Corros. Sci.*, *141* (2018) 18-21.
12. G. Tranchida, M. Clesi, , F. Di Franco, F. Di Quarto and M. Santamaria, *Electrochim. Acta, 273* (2018) 412-423.
13. S. He, D. Jiang and Z.Sun, *Int. J. Electrochem. Sci.,* 13 (2018) 4700 – 4719
14. L. Wang, A. Seyeux and P. Marcus, *Corros. Sci.*, *165* (2020) 108395.
15. I. Bösing, I. Bobrov, J. Epp, M. Baune and J. Thöming, *Int. J. Electrochem. Sci*, *15* (2020) 319-333.

16. J. Hesketh, E. J. F. Dickinson, M. L.Martin, G. Hinds and A. Turnbull, *Corros. Sci.*, *182*, (2021) 109265.
17. Z. Zheng, J. Long, S. Wang, H. Li, J. Wang and K. Zheng, *Corros. Sci.*, *184* (2021) 109382.
18. D. H. Zhang, X. C. Meng, G. Z. Zuo, M. Huang, L. Li, W. Xu, C. L. Li, Z. L. Tang, J. S. Yuan, Y. B. Liu, X. G. Cao and J. S. Hu, *J. Nucl. Mater.*, *553* (2021) 153032.
19. Z. Zhang, J. Tan, X. Wu, E. H. Han, W. Ke and J. Rao, *Corros. Sci.*,*146* (2019) 80-89.
20. B. Dong, X. D. Wen and L. Feng, *Int. J. Electrochem. Sci*,*15* (2020) 10844-10853.
21. J. Moon, T. H. Lee, J. H. Shin and J. W. Lee, *Mater. Sci. Eng., A*,*594* (2014) 302-308.
22. A. Balitskii, O. Krohmalny and I. Ripey, *Int. J. Hydrogen Energy*, *25* (2000) 167-171.
23. E. T. Kim, M. Ishtiaq, J. C. Han, K. K. Ko, H. J. Bae, H. Sung, J. G. Kim, and J. B. Seol, *Scr. Mater.*, *203* (2021) 114112.
24. O. I. Balyts' kyi, *Mater. Sci.*, 3*4* (1998) 97-109.
25. T. Li, J. R. Scully and G. S. Frankel, *J. Electrochem. Soc*., 165 (2018) C484-C491
26. J. Basumatary and R. J. K. Wood, *Wear*, 376 (2017) 1286-1297.
27. A. Gupta and C. Srivastava, *Corros. Sci.*, 194 (2022) 109945.
28. Q. Zhou, J. Jiang, Q. Zhong, Y. Wang, K. Li and H. Liu, *J. alloys compd.*, 563 (2013) 171-175.
29. Y. Shi, B. Yang, X. Xie, J. Brechtl, K.A. Dahmen and P.K. Liaw, *Corros. Sci.*, 119 (2017) 33–45
30. Y. Y. Yang, Y. Y. Liu, M. L.vCheng, N. W.bDai, M.bSun, J. Li, and Y. M. Jiang, *Acta Metall. Sin. (Engl. Lett.)*, 2 (2019) 98-106.
31. Y. Qiao, X. Wang, L. Yang, X. Wang, J. Chen, Z. Wang, H. Zhou, J. Zou and F. Wang, *J. Mater. Sci. Technol.*, 107 (2022) 197-206.
32. M. H .Moayed and R. C.Newman, *Corros. Sci.*, 48 (2006)1004-1018.
33. H. Wu, Y.Wang, Q. Zhong, M. Sheng, H. Du, and Z. Li, *J. Electroanal. Chem.*, 663 (2011) 59-66.
34. X. Leng, Y. Zhang, Q. Zhou, Y. Zhang, Z. Wang, H. Wang and B. Yang,. *Mater. Res. Express*, 5 (2018) 056513.
35. J. Lv, W. Guo and T. Liang, *J. Alloys compd.*, 686 (2016) 176-183.
36. Q. Zhou, S. Liu, L. Gan, X. Leng and W. Su, *Mater. Res. Express*, 5 (2018) 116534.
37. J.B. Lee and S.I. Yoon, *Mater. Chem. Phys.*, 122 (2010) 194e199